EXTREME LOW FREQUENCY MAGNETIC IMAGING METHOD FOR DETECTION OF DEFECT INSIDE WELDING PARTS OF IRON PLATE

Keiji TSUKADA [1)], Teruki HASEGAWA [1)], Mituteru YOSHIOKA [1)], Toshihiko KIWA [1)],

Katsumi INOUE [2)]

Okayama University [1)], 3-1-1 Tsushimanaka, Okayama, JAPAN

Mes Testing & Research Center [2)], 3-1-1, Tamano, Okayama, JAPAN

INTRODUCTION

Detection methods are available for nondestructive tests to examine abnormalities in constructions such as industrial plants, bridge girders, aircraft, pressure vessels, etc. Magnetic measurement employing a search coil that detects inductance change due to eddy current is usually used for the non-destructive evaluation of metals. However, it is limited to identifying surface cracks because of the limitation of the depth of magnetic exposure. Therefore, X-ray inspection or ultra-sound examination is usually used to detect a defect inside the metal. However, these methods have a restricted measurement location and require expertise, respectively. To improve the detection limit of the eddy current NDE, magnetic sensors such as a magnetic resistive (MR) sensor [1-6], Hall sensor [7] or superconductive quantum interference device (SQUID) [8], which can be operated from extremely low frequency, have been used. Another trend of the eddy current NDE is in the application of imaging techniques using a sensor array or scanning. To estimate defect shape, size and position, many numerical and experimental reports have been published [9-11] . First, the eddy current NDE measures the secondary magnetic field from the subject, which is applied by a primary magnetic field. When the eddy current NDE is applied for ferromagnetic materials, the measuring signal becomes more complex. The measuring signal is a mixed signal of the secondary magnetic

field by inducing eddy current and magnetic flux change as a result of the high permeability of the subject. We reported an imaging method measuring the vector component of normal and tangential components to investigate magnetic properties such as eddy current and permeability [1]. In this study, we developed a method and system of magnetic imaging using a magnetic resistive (MR) sensor to detect deeper defects inside the welding part of iron plate. Using this measuring technique operated at extreme low frequency up to a few Hz, we examined the detection possibilities.

EXPERIMENTAL

The measuring system consists of an exposure coil making the magnetic field (z-) component perpendicular to the sample surface, a pair of MR sensors detecting x- and y-magnetic field components, a sample scanning stage, and measuring circuits (Fig. 1). To expose the magnetic field to a wide area of the sample, the radius of the coil was 80 cm and separated 53 cm from the sample. Each signal from the MR sensors detecting x- and y-components was connected to lock-in amplifiers, and they were divided to two phases of the real part and an imaginary part. The exposure coil was driven with an alternating current of 1 A. The system configuration measuring the tangential component produced a highly sensitive measurement of a very weak signal from the subject because the tangential component of the exposed magnetic field at the sensor position was very weak. We reported that the measurement of the tangential component was effective for the current distribution measurement compared with the normal component measurement. The tangential magnetic field distribution reflected the current distribution image because the location of the peak in the tangential component was coincident to the location of the current source. This is the reason why tangential measurement was applied to our eddy current NDT. Iron plate samples without and with a slit-like artificial defect of 50 mm in length inside the welding parts (Fig. 2) were measured. The magnetic field imaging was obtained using multi-point measurement. The sample stage was made from a non-acrylic material. The iron plate on the sample stage was

moved in the x- and y-direction with a 2-mm interval. These samples have a thickness of 8.5 mm and the welding part width was about 10 mm. The defect shape was measured by X-ray, ultra-sound and fracturing observation. Each of the magnetic field vectors at the measuring point was calculated from two parameters of signal amplitude and phase obtained by a lock-in amplifier. The tangential component of the exposure magnetic field was not zero at the sensor position, therefore the measured component included not only the net component from the sample but also the residual component. To obtain the net component from the sample, a vector analysis method was used. First, the residual magnetic vector (signal strength and phase) component was measured, and next the magnetic vector from the sample was measured. The net component was obtained by subtracting the residual magnetic vector from the measured magnetic vector. The measurement of the residual magnetic vector was sufficient only at the first time. Each tangential magnetic component Bx and By, and combined tangential magnetic component $B_{xy}=(B_x^2+B_y^2)^{1/2}$ distributions were imaged. The measurement area at the center of the welding part was 40 mm x 100 mm with a measuring point matrix of 21 x 51 (Fig. 2). The eddy current vector was reconstructed using the following formula in the tangential map:

$$I_{xy} = K(-B_y e_x + B_x e_y)$$

Here, K is a constant and e_x and e_y are the respective unit vectors for the x- and y-axes. The current vector was superimposed in the B_{xy} map.

RESULTS AND DISCUSSION

At the high frequency of 1 kHz, the B_{xy} map of both samples showed a homogenous circulated flow across the welding parts (Fig. 3(a)). The exposed magnetic field area was large compared to the iron plate area. Therefore, the induced eddy current circulated, and the maximum current intensity occurred around the periphery of the quadrate. However, the Bxy map showed a different pattern according to the decrement of the frequency (Fig. 3(b)). The magnetic field intensity at the

welding part was significant at an extremely low frequency. Separate and opposite magnetic fields at both fringes along the welding parts were observed. It is thought that the B_{xy} map reflected not only the eddy current but also the permeability change at the welding part. According to the decrement of the frequency, the eddy current intensity decreases. The welding part has a convex outer surface. Therefore, the magnetic flux was concentrated at the welding part. This caused the increment of the B_{xy} component at both fringes along the welding part. Therefore, the B_{xy} map at the low frequency showed a complex pattern with the magnetic fields caused by the eddy current and magnetic field change by morphological change at the welding part. To analyze the B_{xy} map, each magnetic component map of B_x and B_y was drawn (Fig. 4). Due to the welding part shape, the main magnetic field component was B_x perpendicular to the welding line. The B_x component mainly consisted of the magnetic field change as a result of the morphological change. On the other hand, the B_y component was weak and not significantly affected by the morphological change. Therefore, it is thought that the eddy current change will be easily extracted from the B_y map. In the B_y map at 50 Hz, one magnetic peak is observed at one edge side of Position B of the defect. To investigate the magnetic peak, B_y maps at different frequencies from 5 Hz to 50 Hz were compared (Fig. 5). According to the decrement of the frequency, the observed peak gradually became remarkable. In addition, one more peak at the other edge side of Position A of the defect gradually became remarkable. The distance of the two magnetic peaks was coincident to the length of the defect. However, these peak patterns were slightly different; the lower side peak at Position B showed a circular pattern, and the upper side at Position A showed an elliptic figure. The difference of both peaks was thought to be due to the depth profile of the defect. To investigate the precise depth profile, the sample was observed by the destructive test. Figure 6 shows the cross-sectional profiles at the welding part. A slit-like defect shape of about 3 mm depth was observed across the welding part (Fig. 6(a)). The welding part has a convex outer surface at the front and back side. This shape of the welding part caused the exposed magnetic field focusing and B_x change. Figure 6(b) shows

the cross-sectional profile along the welding part, and the dark part in the figure is the defect part. The defect has a steep edge at Position B. On the other hand, the defect has a gentle slope toward the direction of the edge at Position A. This means that the depth gradually increased toward the direction of the edge at Position A. The eddy current density in a material is not uniform in the depth direction. The skin depth equation given below shows the magnetic field penetration depth.

$$\delta = \frac{1}{\sqrt{\pi f \mu \rho}}$$

The skin depth increases with decreasing frequency. The frequency dependence of the skin depth can explain the different characteristics of each magnetic peak at Position A and B. The magnetic peak at Position A gradually appeared at a lower frequency than that at Position B, and it has an elliptic figure. This was caused by the gradual increment of depth toward Position A. As a result, the frequency dependence of the B_y map was coincident to the defect configuration.

SUMMARY

The magnetic field image inside the ion plate was obtained by extreme low frequency. As a result of abnormality of the tangential magnetic field distribution, especially in the B_y component parallel to the welding line, detection of defects inside the welding parts of the iron plate was enabled.

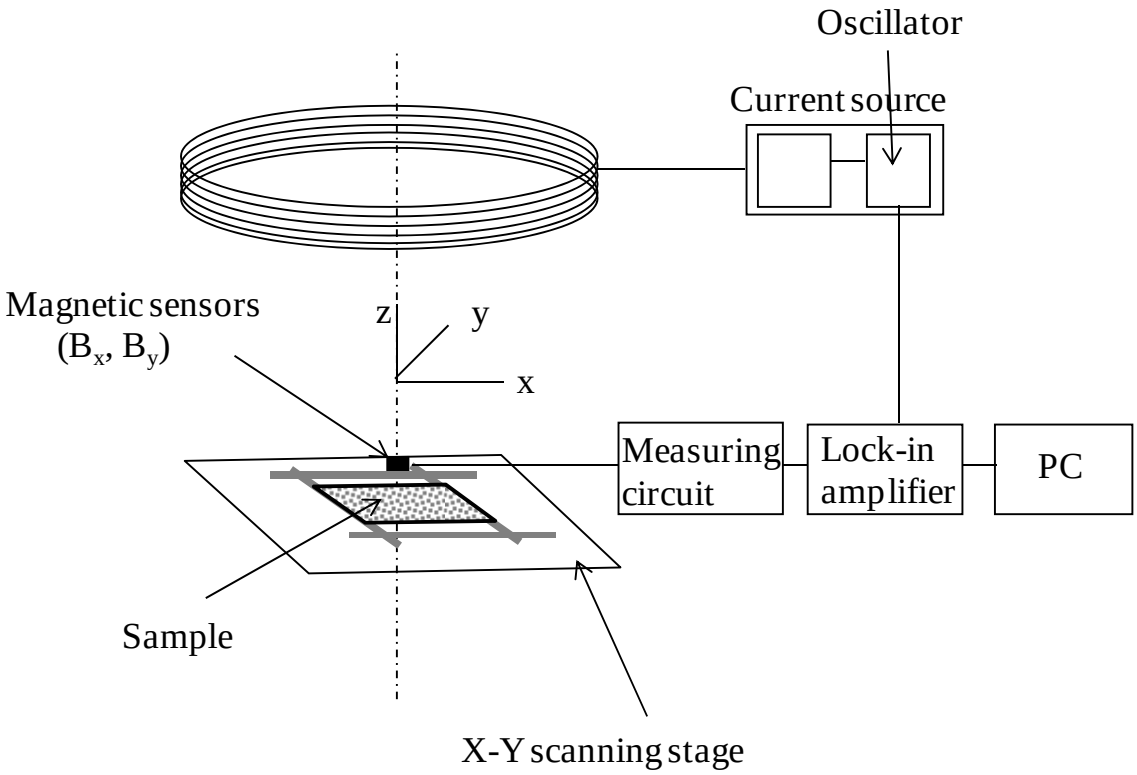

Fig. 1. Schematic diagram of extreme low frequency magnetic imaging system.

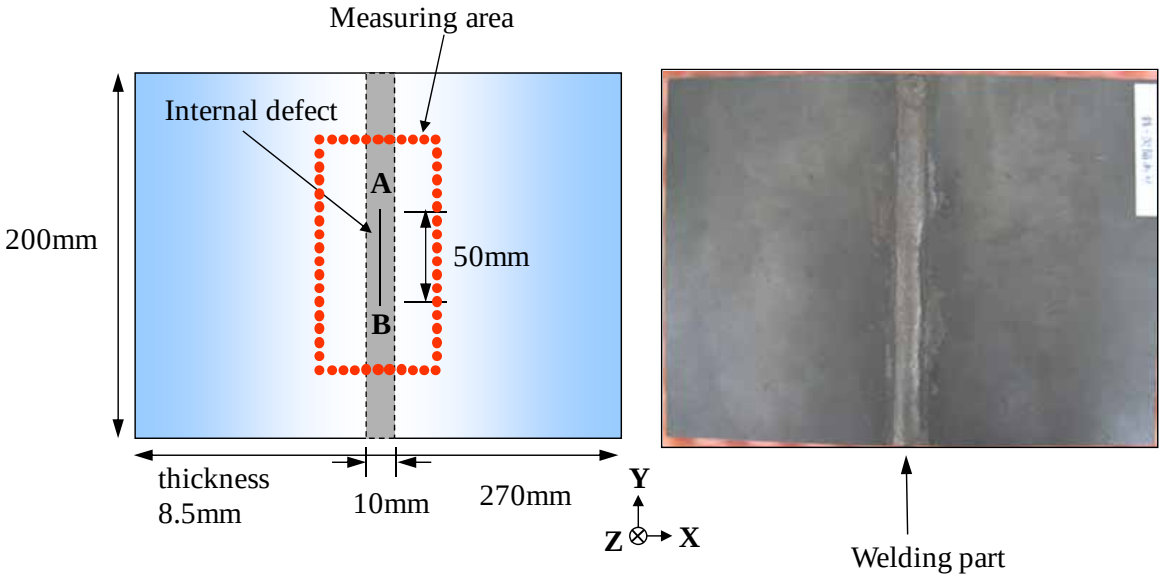

Fig. 2. Iron plate with a slit like artificial defect of 50 mm in length inside the welding parts

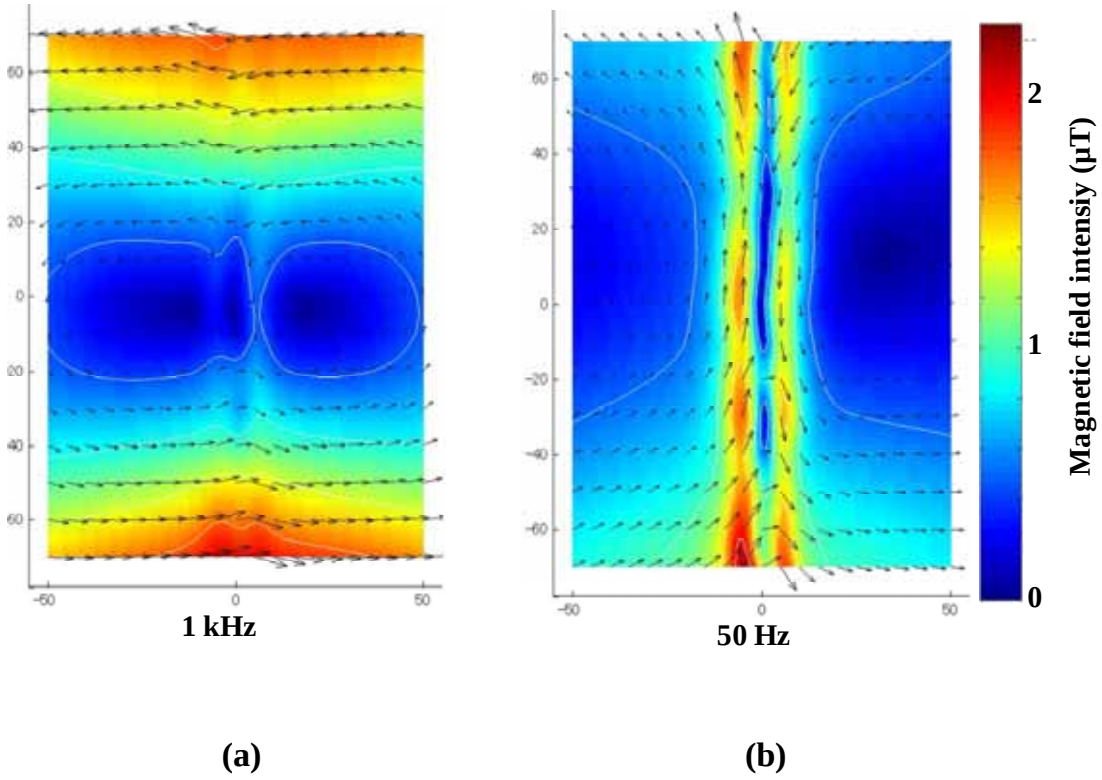

Fig. 3. Frequency dependence of magnetic images of the tangential component B_{xy} at the welding part.

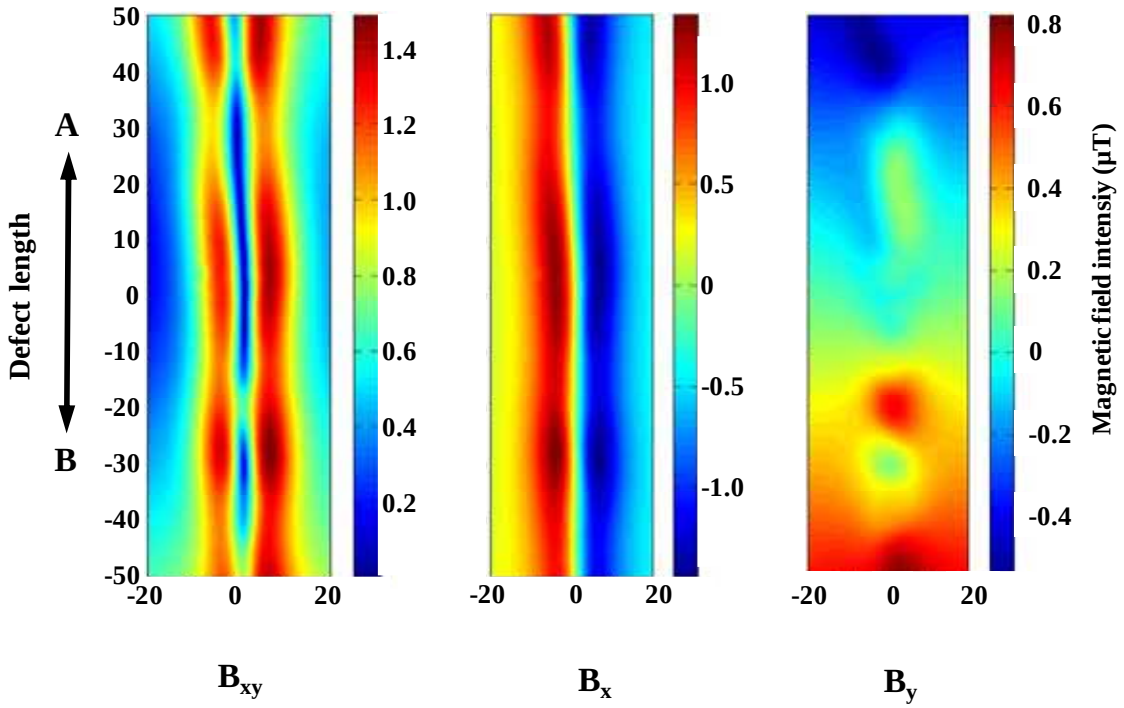

Fig. 4. Each magnetic component at 50 Hz; B_{xy}: tangential component, B_x: x-component, B_y: y-component.

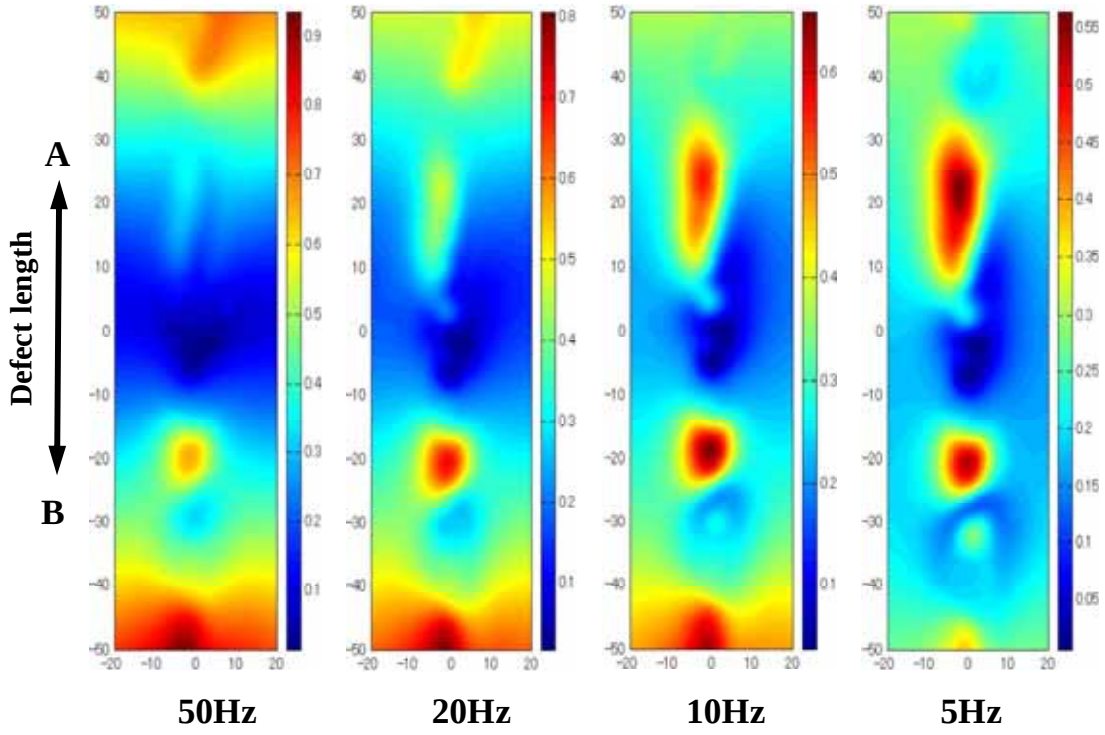

Fig. 5. Frequency dependence of magnetic images of the B_y at the welding part.

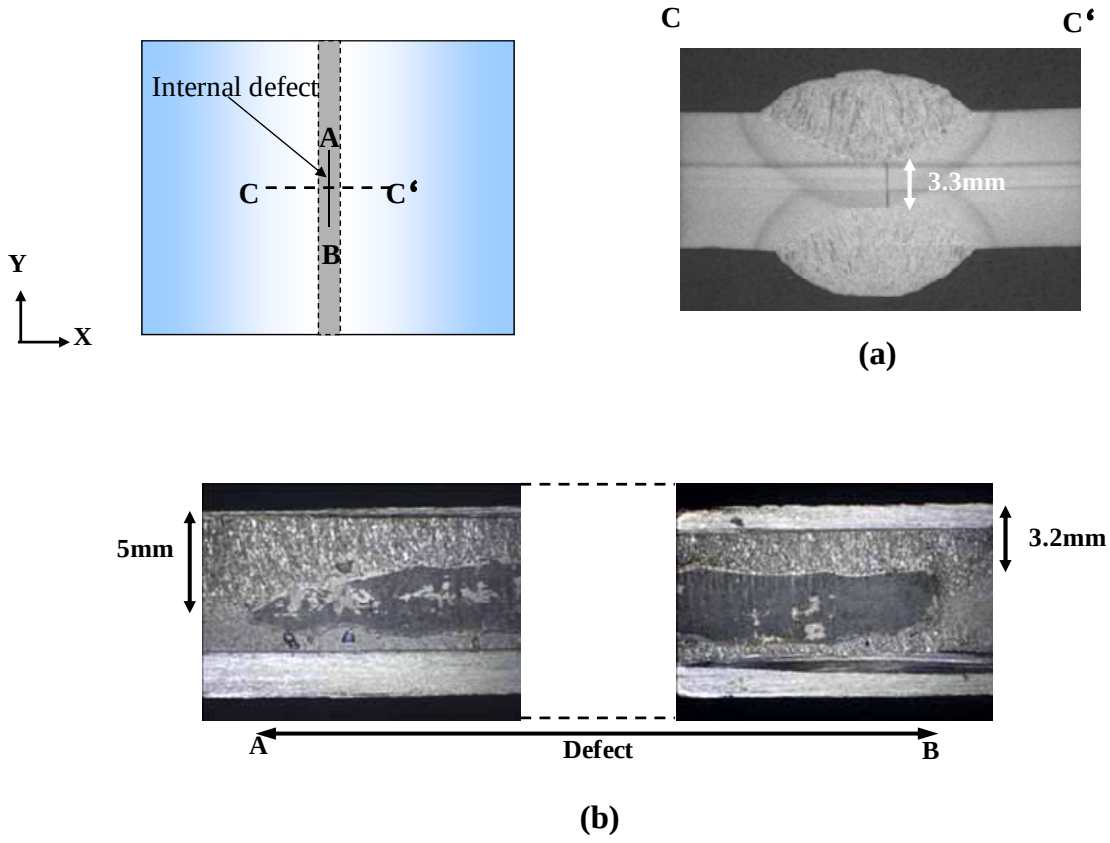

Fig. 6. Cross-sectional configuration of the defect at the welding part, (a) across the welding part, (b) along the welding part.

References

[1] K. Tsukada, T. Kiwa, *Rev. Sci. Instruments* 2006; 77: 063703

[2] T. Kiwa, T. Kawata, K.Tsukada. *Int J Appl. Electromagn Mech* 2007; 25: 447-451.

[3] H. Yamada, T. Hasegawa, Y. Ishihara, T. Kiwa, K. Tsukada. *NDT&E Int* 2008; 41: 108-111.

[4] K. Tsukada, T. Kiwa, T. Kawata, Y. Ishihara, *IEEE Transactions on Magnetics* 2006; 42: 3315-3317

[5] T. Hayashi, H. Yamada, T. Kiwa, K. Tsukada, M. Tamazumi, *J Appl Phys* 2008; 103: 07E923-1-3

[6] T. Hayashi, Y, Kawasaki, H. Yamada, T. Kiwa, M. Tamazumi, K. Tsukada, NDT&E Int 2009; 42: 308-315.

[7] K. Kosmas, Ch. Sargentis, D. Tsamakis and E. Hristoforou. J Mater Process Tech 2005; 161: 359-362.

[8] T. Kiwa, H. Tahara, E. Miyake, H. Yamada, K. Tsukada. IEEE T Appl Supercon 2009; 19: 801-803.

[9] B. A. Auld and J. C. Moulder, J. Nondestruct. Eval 1999; 18: 3-36

[10] V. P. Lunin, Russ J Nondestr Test 2006; 42: 817-822

[11] V. V. Dyakin, V. A. Sandovskii, and S. L. Kaibicheva. Russ J Nondestr Test 2001; 37: 198-206